JGR Solid Earth

RESEARCH ARTICLE
10.1029/2019JB018537

Crustal Composition and Moho Variations of the Central and Eastern United States: Improving Resolution and Geologic Interpretation of EarthScope USArray Seismic Images Using Gravity

H. L. Zhang[1], **D. Ravat**[2], **and A. R. Lowry**[3]

[1]Hubei Subsurface Multi-Scale Imaging Key Laboratory, Institute of Geophysics and Geomatics, China University of Geosciences, Wuhan, China, [2]Earth and Environmental Sciences, University of Kentucky, Lexington, KY, USA, [3]Department of Geosciences, Utah State University, Logan, UT, USA

Key Points:

- Central and eastern U.S. Moho density contrast and velocity-density relationships for crustal and upper mantle V_p/V_s ratios are estimated using gravity data
- Denser sampling of gravity data interpolates seismic models and reduces aliasing of geologic features caused by the USArray station spacing
- High-resolution crustal density variation constrained by seismic information in the central and eastern United States provides detailed information for interpretation

Correspondence to:
H. L. Zhang,
h.l.zhang@cug.edu.cn

Citation:
Zhang, H. L., Ravat, D., & Lowry, A. R. (2020). Crustal composition and Moho variations of the central and eastern United States: Improving resolution and geologic interpretation of EarthScope USArray seismic images using gravity. *Journal of Geophysical Research: Solid Earth*, *125*, e2019JB018537. https://doi.org/10.1029/2019JB018537

Received 13 AUG 2019
Accepted 22 FEB 2020
Accepted article online 26 FEB 2020

Abstract EarthScope's USArray Transportable Array has shortcomings for the purpose of interpreting geologic features of wavelengths less than the Transportable Array station spacing, but these can be overcome by using higher spatial resolution gravity data. In this study, we exploit USArray receiver functions to reduce nonuniqueness in the interpretation of gravity anomalies. We model gravity anomalies from previously derived density variations of sedimentary basins, crustal V_p/V_s variation, Moho variation, and upper mantle density variation derived from body wave imaging informed by surface wave tomography to estimate V_p/V_s. Although average densities and density contrasts for these seismic variations can be derived, the gravity anomalies modeled from them do not explain the entire observed gravity anomaly field in the United States. We use the unmodeled gravity anomalies (residuals) to reconstruct local variations in densities of the crust associated with geologic sources. The approach uses velocity-density relationships and differs from density computations that assume isostatic compensation. These intracrustal densities identify geologic sources not sampled by and, in some cases, aliased by the USArray station spacing. We show an example of this improvement in the vicinity of the Bloomfield Pluton, north of the bootheel of Missouri, in the central United States.

1. Introduction

The EarthScope program has led to significant advances in geophysical understanding of seismic velocity and electrical resistivity variations in the crust and upper mantle of the United States and their implications for Earth history and dynamics (e.g., Bedrosian, 2016; Liu & Hasterok, 2016; Long et al., 2016; Love et al., 2016; McGlannan & Gilbert, 2016; Porter et al., 2016; Schmandt et al., 2015; Shen & Ritzwoller, 2016). Within the footprint of the seismic experiment, USArray's Transportable Array (TA), this has led to better understanding of seismic velocity variations at a spatial resolution of ~70 km and finer resolution where the spacing was supplemented with Flexible Arrays targeting particular geologic problems (e.g., Yang et al., 2017). The TA has produced estimates of variations in crustal and upper mantle V_p/V_s and impedance structure through receiver function analysis (Frassetto et al., 2011; Levin et al., 2016; Lowry & Pérez-Gussinyé, 2011; Ma & Lowry, 2017; Miller et al., 2014; Parker, 2013; Pollitz & Mooney, 2016; Stanciu et al., 2016; Tape et al., 2012; Thurner et al., 2015; Yeck et al., 2013; Yuan et al., 2010), crustal imaging from other seismic observables (Kiser et al., 2016; Schmandt et al., 2015), and variations in the upper mantle using Rayleigh wave and body wave tomography (Biryol et al., 2016; Buehler & Shearer, 2016, 2017; Nyamwandha et al., 2016; Schmandt & Humphreys, 2010; Schmandt & Lin, 2014; Workman et al., 2017).

Seismic investigations are primarily sensitive to velocity, which have well-established ambiguities introduced by source-receiver sampling of the Fresnel zones sensed by the waves (Heeszel et al., 2016; Savage et al., 2016). These ambiguities can be mitigated by combining with variations in the gravity field that arise from lateral density variations, owing to various physical state properties that correlate rock density and elastic properties. In the western United States, Lowry and Pérez-Gussinyé (2011) showed that the trade-off between the crustal seismic V_p/V_s and the crustal thickness can be reduced significantly by constraining automated receiver function analyses (Crotwell & Owens, 2005; IRIS DMC, 2010) with gravity anomalies and that one could also derive the average density contrast at the Moho, the mean derivative of

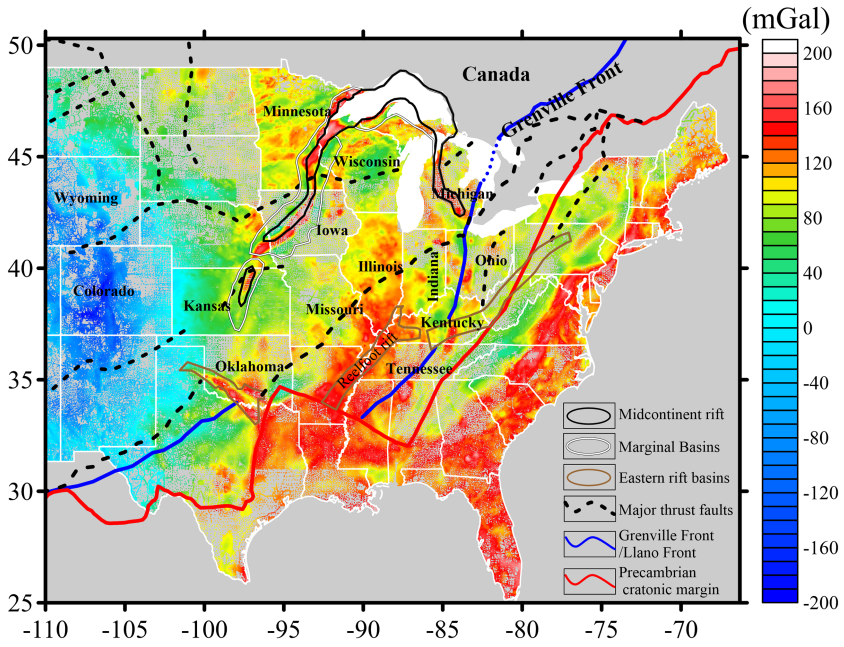

Figure 1. Gravity observations in the central and eastern United States from the Pan-American Center for Earth and Environmental Studies (PACES). Most tectonic boundaries are from Whitmeyer and Karlstrom (2007); the Midcontinent Rift System is a modified version of Van Schmus and Hinze (1985).

density with respect to V_p/V_s in the crust, and the coefficient of thermal expansion leading to the gravity anomalies from lateral density variations due to temperature variations in the Earth's crust and mantle.

Over the last century, gravity variations of the Earth have been investigated globally from a large variety of platforms (ground, airborne, marine, and satellite) for diverse applications to environmental, geological and geophysical problems. In regional ground gravity surveys in the United States, station spacing varies from hundreds of meters to a few tens of kilometers, but since these data represent a continuous potential field, they can be gridded at average spacing of 6–10 km or less depending on the region. The denser sampling by gravity observations permits investigation of smaller-scale geological features including sedimentary basins, igneous plutons, salt domes, stratigraphic variations, and Moho variations at scales that are unsampled (e.g., the Great Lakes and offshore regions) or aliased by the 70 km TA spacing. Because the non-uniqueness inherent in interpretation of gravity anomalies is reduced significantly by EarthScope seismic data, we show in this paper that combining the strengths of the two methods and their data sampling leads to more realistic density contrast variation and first-order improvement in estimates of the compositional variation of the Earth's crust in the midcontinent region of the United States (Figure 1).

2. Methods and Data Sets

Velocity-density relationships in the Earth's lithosphere are affected by several factors including chemistry, mineralogy, pressure, temperature, and partial melting states (Barton, 1986; Brocher, 2005; Christensen & Mooney, 1995; Ludwig et al., 1970; Ravat et al., 1999). The variation of these factors with chemistry, for example, is reflected in an opposite sign of the relationship of V_p/V_s to density for crustal and mantle rocks (Figure 2). There is significant scatter in the measurements and, thus, a single V_p/V_s-density relationship may not be applicable even in a single lithospheric setting and may require regional modifications.

In this study, we begin with κ_c (defined as the crustal V_p/V_s) and crustal thickness in the central and eastern United States (Figure 3) derived from the method of Lowry and Pérez-Gussinyé (2011), which improves upon the V_p/V_s and crustal thickness estimated by the EarthScope Automated Receiver Survey (EARS) by using constraints from gravity anomalies. These are supplemented with CRUST1.0 (Laske et al., 2012) crustal thickness estimates outside the USArray footprint. The seismic imaging does not take into account other crustal and upper mantle interfaces because that requires additional information not included in single-layer

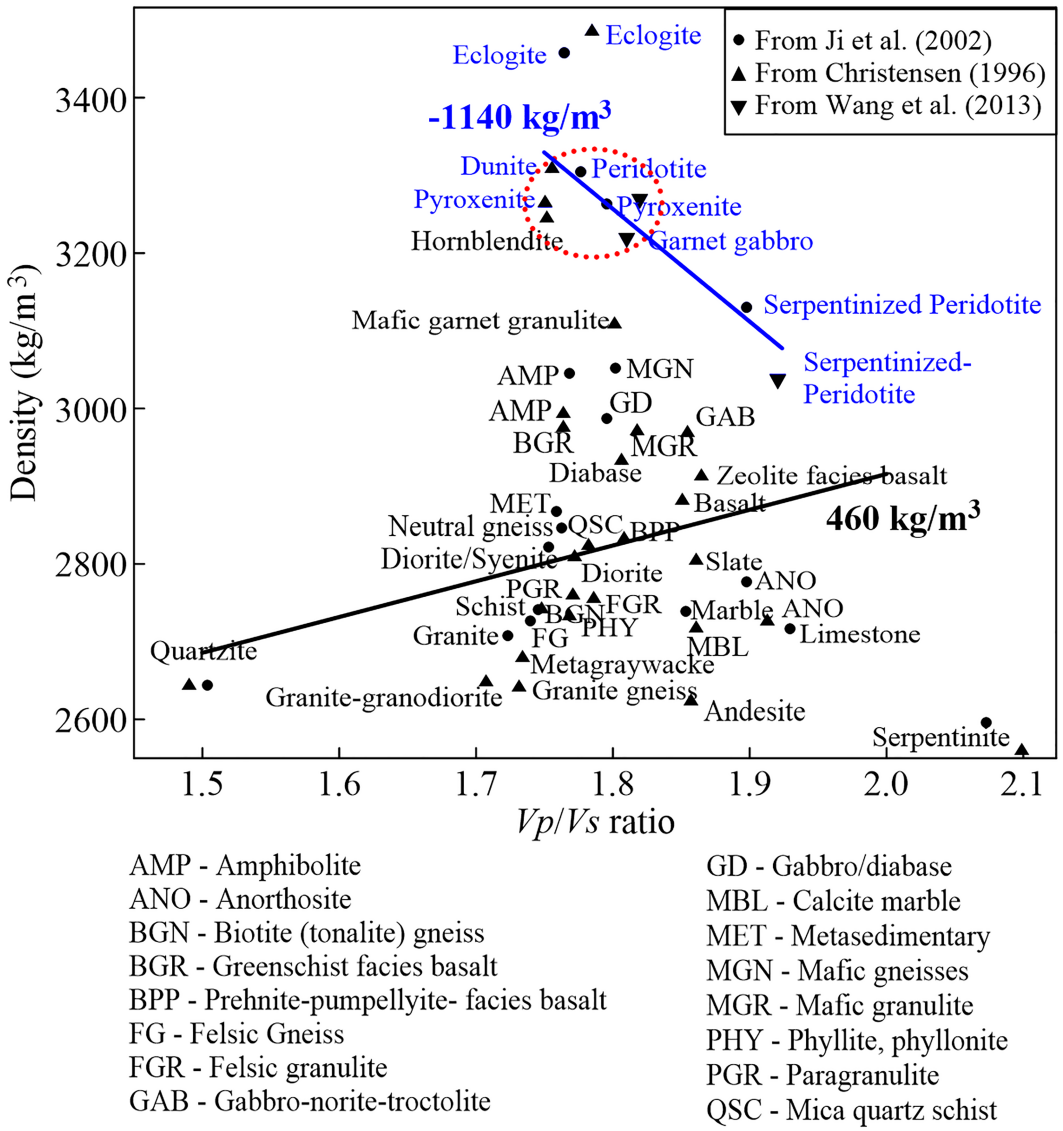

Figure 2. Average densities versus average V_p/V_s for various rock measurements. The black line shows the crustal compositional density parameter, $\partial\rho/\partial(V_p/V_s) = 460$ kg/m^3, estimated by Lowry and Pérez-Gussinyé (2011) in the western United States. The blue line indicates a derivative initially used to convert upper mantle V_p/V_s to density for testing in this study. The dashed red ellipse encompasses unaltered mantle rocks. Filled circles and inverted triangles are data from Ji et al. (2002) and Wang et al. (2013), respectively.

H-κ receiver function stacks afforded by EARS (e.g., Ma & Lowry, 2017). Since sedimentary basins could contribute significantly to gravity anomalies, we calculate basin anomalies (Figure 4) combining basin thickness estimates from several sources (Ellett & Naylor, 2016; Hinze et al., 1982; Laske et al., 2012; Mooney & Kaban, 2010) with basin density-depth variations suggested by Mooney and Kaban (2010). We also model the gravity effect of mantle density variations using dV_p and dV_s variations from Schmandt and Lin (2014). To model the gravity effects, we require the Moho density contrast, $\Delta\rho_{Moho}$, and partial derivatives of density with respect to the crustal V_p/V_s (κ_c), $\frac{d\rho}{d\kappa_c}$, and the upper mantle V_p/V_s (κ_m), $\frac{d\rho}{d\kappa_m}$. It is possible to estimate first order conversion parameters in the crystalline crust and the uppermost mantle from relationships of the seismic properties to gravity anomalies.

The EarthScope USArray spacing imposes limitations on the EARS-derived V_p/V_s and crustal thickness. Narrow features with <70 km width are inadequately sampled or aliased in places, including the Midcontinent rift (Figure 1, with the western arm through Lake Superior and the states of Wisconsin,

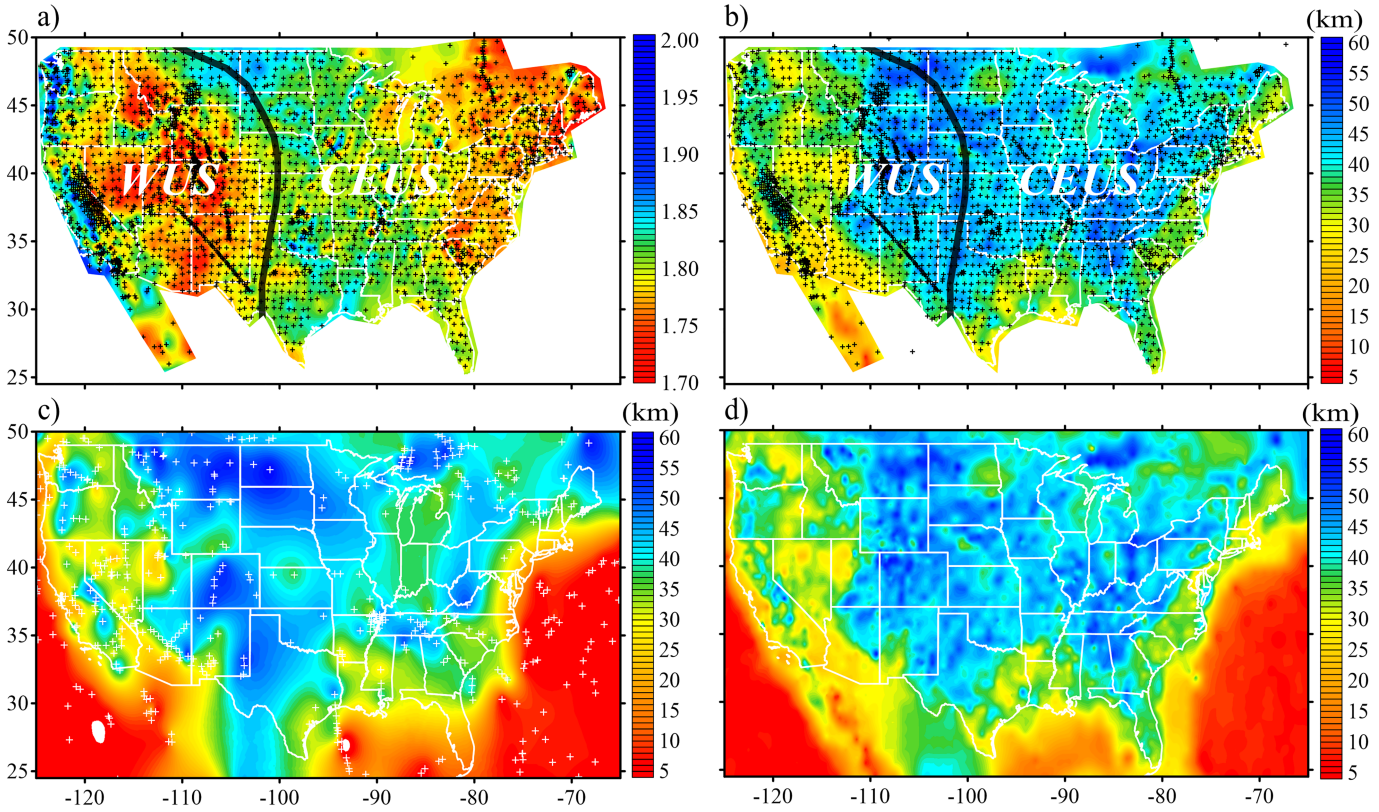

Figure 3. Gravity-constrained (a) crustal V_p/V_s and (b) crustal thickness from the method of Lowry and Pérez-Gussinyé (2011), combined with global crustal thickness from Laske et al. (2012) in regions not sampled by USArray. The black crosses show locations of stations in the EARS data product. WUS and CEUS indicate western United States and central and eastern United States, respectively. (c) The Moho depth from seismic refraction data (Mooney & Kaban, 2010) where white crosses indicate the data points. (d) Combined Moho depth from (b) and (c). See text for details.

Minnesota, Iowa, and Kansas, and the eastern arm through Michigan), Southern Oklahoma aulacogen, Proterozoic sutures like the Grenville Front (through Ontario, Canada, to Lake Erie and states of Ohio, Kentucky, Tennessee), and small features such as igneous plutons. We examine a prominent example of aliasing in more detail in the discussion section. Moreover, receiver function imaging is notoriously error prone in regions with thick sedimentary packages, and high-velocity basal layers that may be

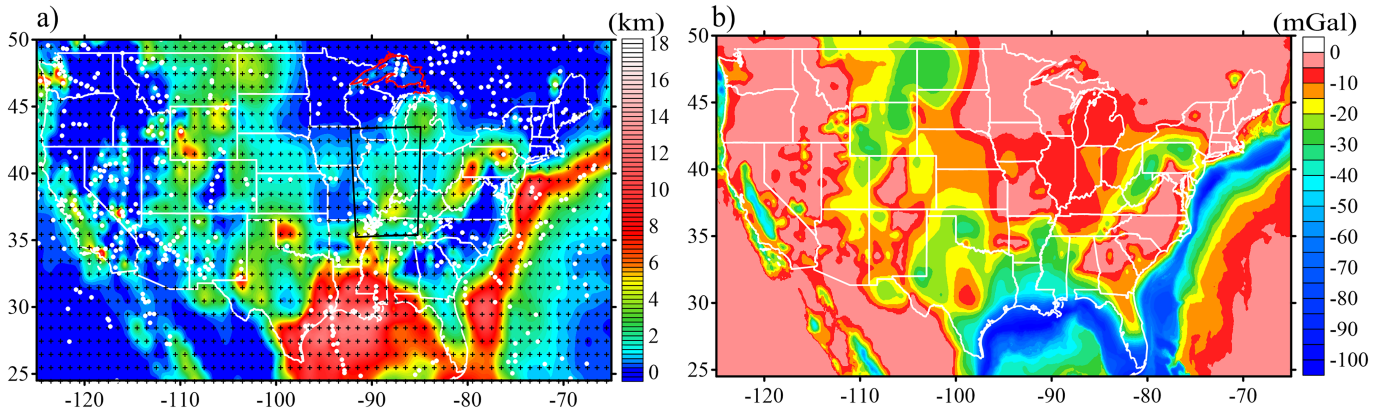

Figure 4. (a) Sedimentary basin thickness from Mooney and Kaban (2010) over North America (filled white circles), Ellett and Naylor (2016) high-resolution (5 km spacing) data in the Illinois basin region (shown by the black box), the digitized isopach map of the Jacobsville sandstone from Hinze et al. (1982) (shown by the red polygon over Lake Superior), and the global sedimentary thickness from Laske et al. (2012) (black pluses) over the rest of the region. (b) Gravity anomalies from the sedimentary basin fill.

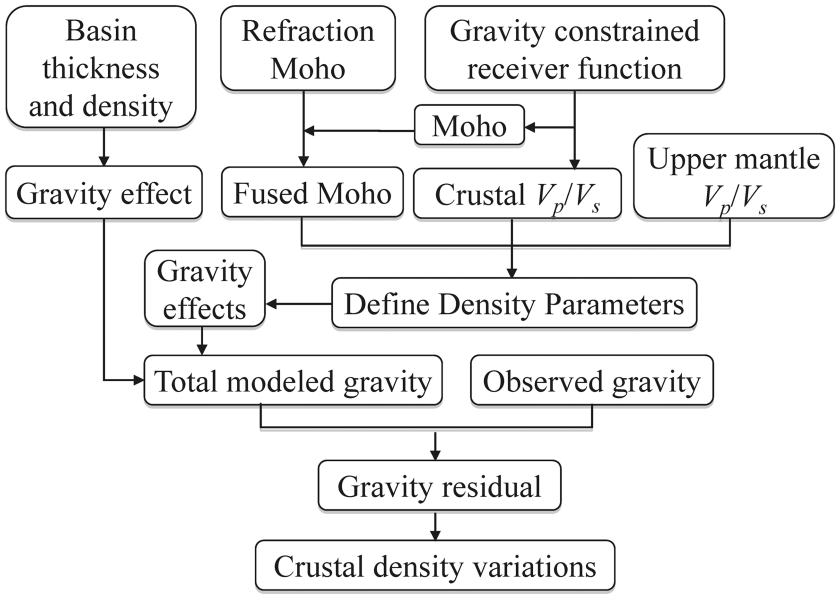

Figure 5. Flow chart of the steps leading up to the calculation of crustal density variation.

present are sometimes misattributed to the mantle. One example occurs in the northernmost Mississippi embayment, where the Moho lies at a depth of 40–45 km (based on long reversed refraction profiles, Catchings, 1999; Mooney et al., 1983; Yang et al., 2017), but the gravity-constrained receiver function imaging estimates crustal thicknesses of 36–38 km, corresponding to the top of a high-velocity basal crustal layer (Figure 3c). The seismic refraction sampling is sparse (Figure 3c) but consistent with the broad features of the gravity-constrained and corrected Moho depth, and thus, the two data sets can be combined while honoring refraction results in the regions of disagreement. In our merged Moho data set, estimates from the method of Lowry and Pérez-Gussinyé (2011) within 70 km of seismic refraction observations (Mooney & Kaban, 2010) are removed. We then grid the merged data set to obtain the "fused" Moho depth (Figure 3d).

We forward model gravity effects layer by layer using the Fourier method of Parker (1973), where we discretize layers at 1 km depth intervals from the surface to the deepest Moho estimate. The remaining upper mantle is modeled from the base of Moho topography to 230 km using V_p/V_s at corresponding depths obtained from the dV_p, dV_s from Schmandt and Lin (2014), which are multiplied by the AK135 reference model (Kennett et al., 1995) before calculating the seismic velocity ratio. To avoid edge effects, all layers have been extended beyond the USArray receiver function stations by at least 260 km in all directions including the modeling of oceanic density variations.

Figure 4a depicts the thickness of sedimentary basins from the refraction data from Mooney and Kaban (2010) over North America augmented with Ellett and Naylor (2016) high-resolution (5 km spacing) data in the Illinois basin region, the digitized isopach map of the Jacobsville sandstone from Hinze et al. (1982) in the Lake Superior region, and the global sedimentary thickness from Laske et al. (2012) over the rest of the region. The density-depth curves for six typical geological provinces within North America from Mooney and Kaban (2010) are used in this modeling. Gravity anomalies produced by sedimentary basins (Figure 4b) also are modeled using the Fourier method of Parker (1973) and are substantial.

The major steps of the procedure are illustrated as a flow chart in Figure 5. After calculating the seismic structure-derived and basin models of gravity, "remainder" crustal density variations were calculated from the residual gravity anomaly (i.e., observed minus forward-modeled gravity anomalies) by iteratively inverting the Fourier domain gravity anomaly expression within the thickness of the crust using the method of Caratori Tontini et al. (2008). Their expression for the density is

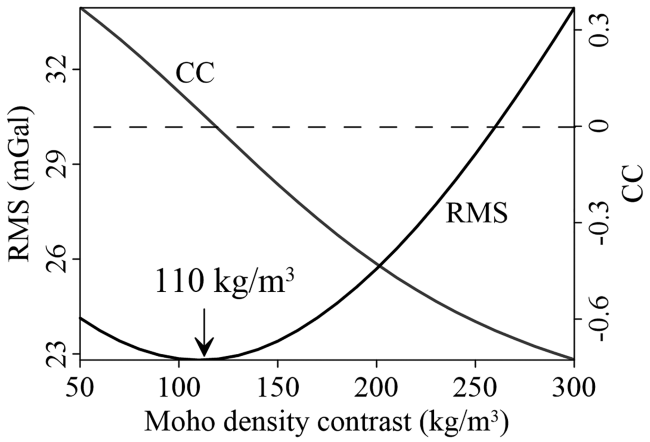

Figure 6. The RMS of the final residual after subtraction of the sedimentary and the Moho gravity model and the correlation coefficient (CC) between the residual and the modeled gravity anomaly for a range of Moho density contrasts. The minimum correlation corresponds to the derived Moho density contrast in the study. The procedure is reasonable when the correlation between the crustal V_p/V_s and crustal thickness is minimal.

$$\widetilde{\rho_s} = \frac{2\widetilde{\Delta g}}{2\pi G \cdot e^{K_r \cdot z_0}} - \sum_{n=2}^{\infty} \frac{(-|K_r|).^{n-1}}{n!} \rho_s \widetilde{P_{n-1}(z_1, z_2)}, \quad (1)$$

where all tilded quantities are Fourier transform representations of spatial variations; $\rho_s = \rho(z_1 - z_2)$ is the equivalent surface density of the layer with density ρ; z_0, z_1, and z_2 are the observation surface and the upper and lower interfaces, respectively; $K_r = \sqrt{K_x^2 + K_y^2}$ is the wavenumber; Δg is the gravity anomaly; G is the universal gravitational constant; n is the exponent of Taylor series expansion in the Parker method; and $P_{n\text{-}1}$ is a polynomial of degree $n - 1$. The iterations are carried out until convergence is achieved (Caratori Tontini et al., 2008).

3. Estimation of Density Parameters

In principle, the residual between the observed and modeled gravity anomalies should not correlate with the modeled anomaly, because otherwise different density parameters would better explain the observed gravity anomalies. We do not use density parameters derived from the joint inversion of seismic and gravity, because that approach used stochastic inversion for density parameters (Ma & Lowry, 2017), which biases density parameter estimates toward a laboratory measurement-derived expectation. Since the V_p/V_s-density parameters are average parameters from regression over the entire region analyzed, they do not explain the actual observed variations in the gravity field caused by local variations in density. The optimal density parameters will also differ from those estimated for the joint inversion because this study examines a different region, incorporates crustal thicknesses from seismic refraction data and CRUST1.0, and also uses mantle V_p/V_s as a proxy for mantle density rather than the thermal model described in Ma and Lowry (2017). Hence, we estimate new parameters that minimize the residual gravity anomaly (i.e., observed minus modeled anomaly) by using the root-mean-square (RMS) of the residual gravity.

Using the V_p/V_s-density relationship for mantle rocks shown by the blue line in Figure 2 results in $\Delta\rho_{Moho}$ ~ 270 kg/m^3 and $\frac{d\rho}{d\kappa_c}$ ~ 70 kg/m^3 in central and eastern United States, with a residual gravity RMS (55.8 mGal) larger than that of the observed gravity RMS (28.1 mGal) and a high correlation coefficient between the modeled gravity and the residual field (−0.92). This implies that the V_p/V_s-density relationship for mantle rocks shown in Figure 2 is ill suited to the central and eastern United States. Inspection of the "mantle" rocks in the velocity-density relationship in Figure 2 reveals eclogites and serpentinites (hydrated mantle peridotites), which are unlikely to be found in the central and eastern U.S. mantle. Thus, instead of using the laboratory-derived mantle V_p/V_s-density relationship from Figure 2, we chose to determine the mantle V_p/V_s-density factor and the Moho density contrast in the following manner. First, we minimize RMS of the residual gravity to determine the Moho density contrast (refer to Appendix A for details). There is no significant correlation between the crustal V_p/V_s and the crustal thickness (see Figures 3a and 3d), and thus, using the minimum RMS of the residual between the observed and the combined gravity from all other modeled effects to determine the Moho density contrast is reasonable. As shown in Figure 6, the minimum RMS yields $\Delta\rho_{Moho}$ ~ 110 kg/m^3 with a low correlation coefficient (0.03) between the modeled Moho gravity anomaly and the residual gravity. This value is less than the already-low Moho density contrasts estimated by Schmandt et al. (2015) and Ma and Lowry (2017) and much less than the 400 kg/m^3 typically estimated for continental crust (Christensen & Mooney, 1995; Kende et al., 2017). To estimate the crustal and mantle $\frac{d\rho}{d\kappa_c}$ and $\frac{d\rho}{d\kappa_m}$, we use the RMS of the final residual for a range of $\frac{d\rho}{d\kappa_c}$ and $\frac{d\rho}{d\kappa_m}$. The minimum RMS results in $\frac{d\rho}{d\kappa_c}$ ~ 300 kg/m^3, and $\frac{d\rho}{d\kappa_m}$ ~ 30 kg/m^3 (Figure 7). These parameters are significantly different for the western United States as shown in Figure 3, where , $\Delta\rho_{Moho}$, $\frac{d\rho}{d\kappa_c}$ and $\frac{d\rho}{d\kappa_m}$ are estimated at 70, 1,180, and −100 kg/m^3, respectively. The differences likely reflect warmer uppermost mantle (Schutt et al., 2018) and removal of western U.S. lower crustal garnet phases by hydrous melting (Ma & Lowry, 2017; Schmandt

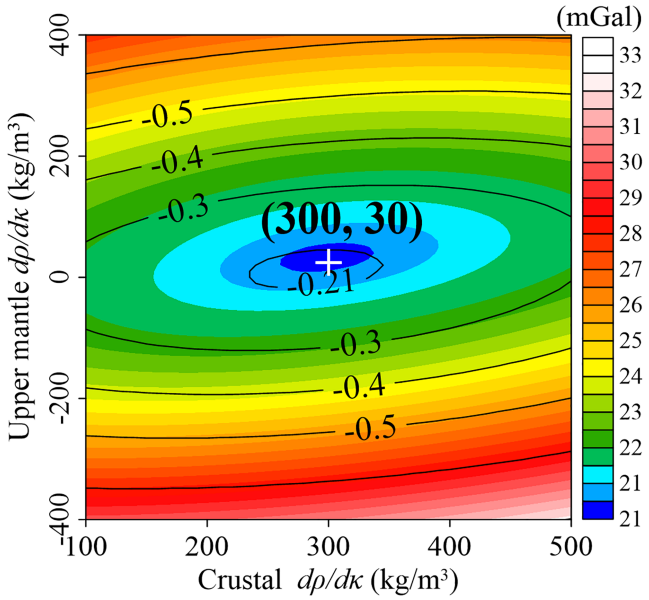

Figure 7. Determination of $\frac{d\rho}{dx_c}$ and $\frac{d\rho}{dx_m}$ for the central and eastern United States. The color contour map shows the RMS of the final residual after subtracting the sedimentary gravity model, the Moho gravity model, the crustal V_p/V_s gravity model, and the upper mantle gravity model. The black contours show the correlation coefficient between the final residual and the modeled gravity anomaly. The minimum correlation coefficient and the minimum RMS indicate the derived $\frac{d\rho}{dx_c}$ and $\frac{d\rho}{dx_m}$.

et al., 2015). The western U.S. relationships were discussed in the study of Lowry and Pérez-Gussinyé (2011), whereas our present study is focused on the central and eastern United States.

The modeled gravity anomalies from crustal V_p/V_s, the Moho depth, and the mantle V_p/V_s using these parameters are shown in Figures 8a–8c, respectively. Figure 8d shows the total modeled gravity from the above three modeled anomalies combined with the sedimentary basin gravity model. Figure 9 depicts the observed Bouguer gravity field and the residual after subtracting modeled anomalies shown in Figure 8d from the observed field. The RMS of the residuals is 21.1 mGal (lower than the observed gravity field RMS), and the correlation coefficient between the total modeled gravity and the residual field, which is one of our criteria in deriving the density parameters (Figure 7), is understandably lower for the model of the present study (−0.20). The nonzero cross correlation with the final residual is an indicator that the final residual is partly correlated with crustal thickness, which implies that some higher density rocks could exist in the crust. We argue later for the presence of eclogite in the deepest part of the crust in regions where crust is unusually thick (>50 km).

The residuals between observed and modeled gravity anomalies suggest that not all of the density variation is encompassed by the seismic-derived parameters, and thus, a further iteration to the density model is possible. In fact, we show later that this iteration is quite important in reducing/removing aliasing of features by the 70 km spacing of USArray's TA. One could invert such a residual field using equation (1) to obtain a density correction for the previously modeled crystalline crust. However, there is no unique way of partitioning the residuals into crustal and mantle variations without further constraints. The most reasonable approach is to use only the longer-wavelength portion of the residual gravity field to correct mantle density, as that is more likely to be dominated by deeper density variations. We found that wavelengths of the residual gravity field shorter than 150 km correspond to many geologically identifiable crustal features in the central and eastern United States.

We justify the filtering approach for the separation of crustal and mantle contributions as follows: Because the mantle variation, as a result of its greater depth, is unlikely to produce short-wavelength gravity anomalies, we can examine various thresholds for filtering and discard those which assign variations to the mantle that are known to be crustal in origin based on geologic or geophysical observations. We found that the residual field of wavelength >150 km leaves behind the least contribution that can be ascribed to the known crustal geologic features, and 150 km is also close to the Nyquist wavelength of the USArray's TA. The only identifiable crustal gravity feature that remains in the >150 km wavelengths of the residual field is a large-scale feature associated with the eastern part of the Midcontinent rift in Michigan. Thus, we use the short wavelengths (high pass of 150 km) of the residual field in Figure 9b to obtain the bulk density correction term of the crystalline crust. The corrected bulk density is shown in Figure 10.

4. Discussion

EarthScope seismic information affords useful constraints on the density variations responsible for gravity anomalies (Lowry & Pérez-Gussinyé, 2011; Ma & Lowry, 2017; Schmandt et al., 2015), but the 70 km spacing of USArray's TA can alias crustal geologic features. The residual gravity anomaly from seismically constrained models such as ours has reduced nonuniqueness of gravity and hence has short-wavelength information that can be used to correct for crustal structure missed by seismic imaging.

The steep mantle V_p/V_s-density relationship of −1,140 kg/m^3 shown by the blue line in Figure 2 leads to a large model anomaly that produces a mirrored large residual anomaly and thus is implausible. A closer examination of rocks in the regression suggests that the slope is indeed conditioned by deep crustal mafics (eclogites, garnet gabbro, and hornblendite) and serpentinized olivines that are unlikely to contribute

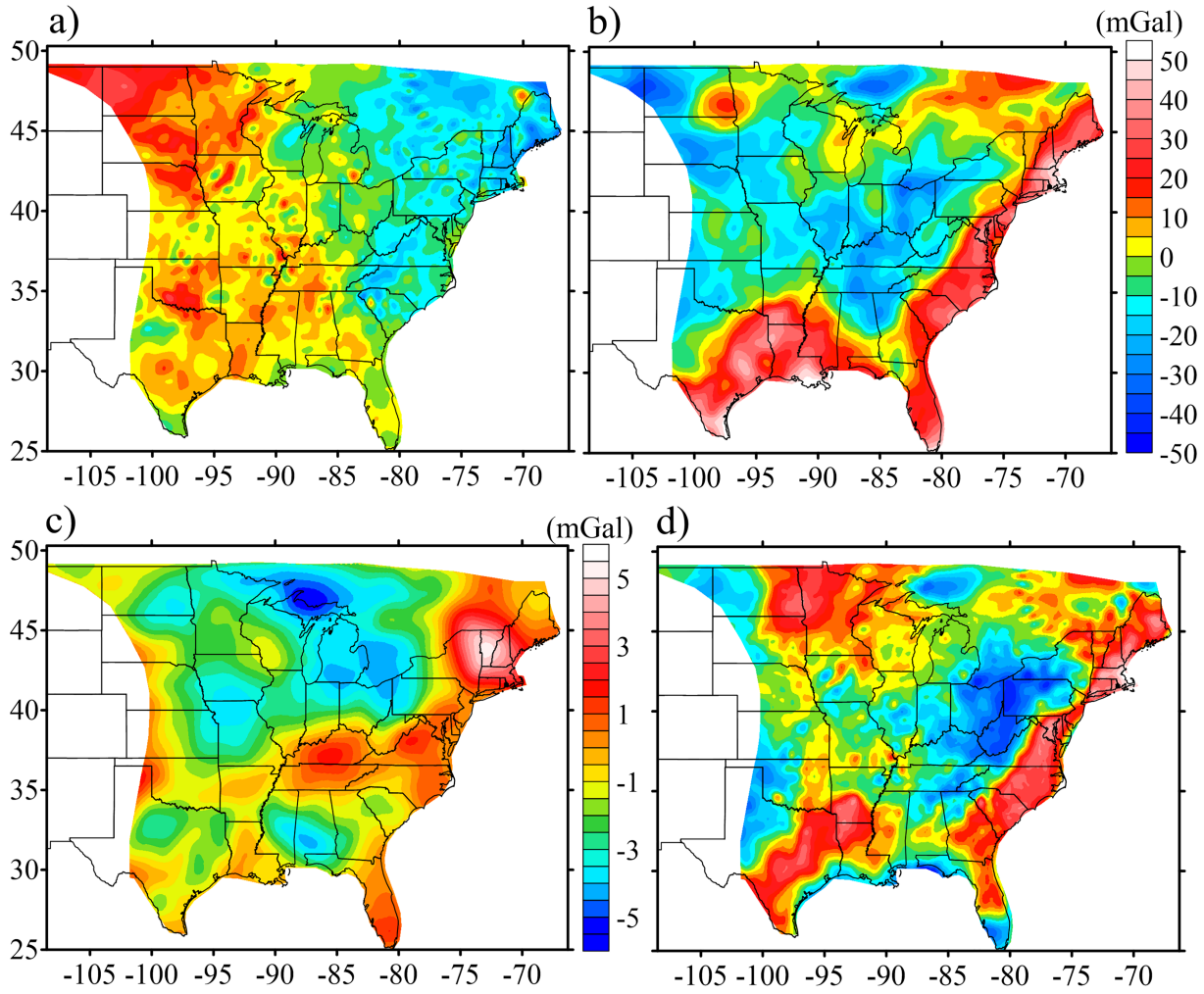

Figure 8. (a) Modeled gravity effect from crustal V_p/V_s. (b) Modeled gravity effect from Moho topography. (c) Modeled gravity effect from upper mantle V_p/V_s. (d) The total modeled gravity including contributions from sedimentary basins (Figure 3b), the crustal V_p/V_s, the Moho topography, and the upper mantle V_p/V_s. Note that (a), (b), and (d) have the same color bar (shown next to panel b).

significantly to density variation in cratonic mantle lithosphere. If we exclude those rocks, the remaining mantle rocks (peridotites and dunites) are relatively few and show poor correlation. Mineral physics (e.g., Cammarano et al., 2003) suggests both chemistry and temperature contribute to the relationship of κ_m to density, with anelasticity effects dominating the relationship. This is consistent with the very small V_p/V_s-density parameter that best fits the data (30 kg/m^3).

The most important assumptions of our procedure are that relationships of V_p/V_s to density are linear and that a single density parameter may represent the entire region. In view of the variation of the gravity field residual (Figure 9b), these assumptions cannot be correct. Yet seismic velocity is theoretically as well as empirically related to density of materials (Birch, 1960, 1961; Christensen & Mooney, 1995), and thus, our approach is reasonable to a first order. This approach also leads to reduction of the RMS of residuals between the observed and the total modeled gravity anomalies.

This study relies heavily on velocity-density relationships, and hence, our approach is very different than computing densities with an assumption of isostatic compensation. The assumption of 100% Airy isostasy typically used in calculating isostatic gravity anomalies is not justified for the central and eastern United States, as large regions of low-relief topography have significant Moho depth variations. Moreover, estimates of the effective elastic thickness, T_e, of the region generally exceed 40 km with some regions reaching typical

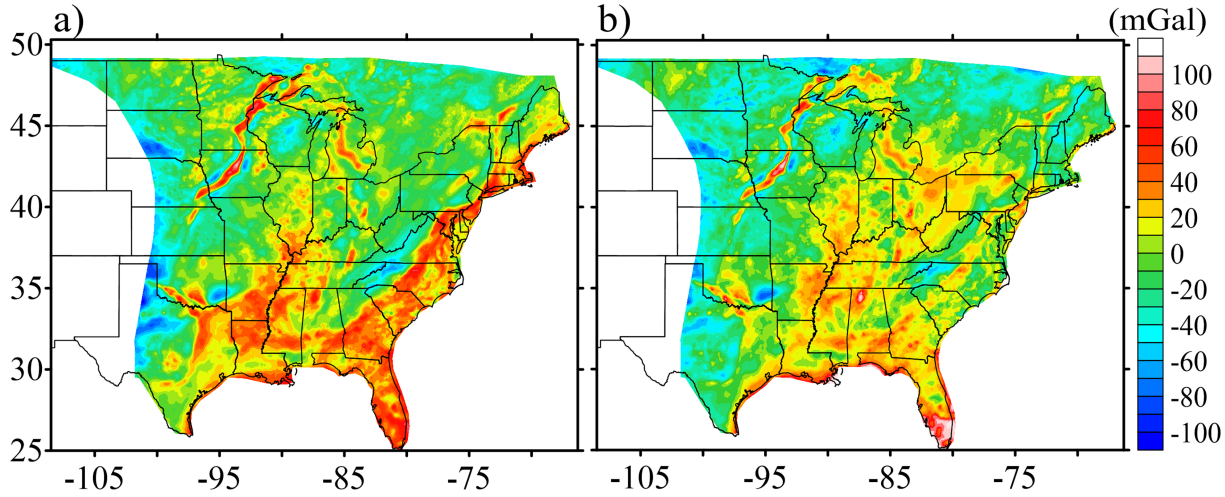

Figure 9. Observed Bouguer gravity anomaly (a) and the residual between observed and modeled anomaly (b).

cratonic values in excess of 100 km (Bechtel et al., 1990; Kirby & Swain, 2009). For a T_e of 40 km, the isostatic response is less than 1% of Airy at wavelengths less than 150 km (and would be even smaller for higher T_e). Hence, flexural isostasy is negligible on the scales of interest in this analysis because loads predominantly are supported by lithospheric stress.

We show an example of geologic aliasing using the gravity anomaly associated with the Bloomfield Pluton, just north of the bootheel of Missouri (36.75°N, 89.75°W) near the New Madrid seismic zone. None of the USArray or New Madrid regional network stations are located atop the pluton, and thus, the V_p/V_s variation associated with the pluton is split into a higher V_p/V_s feature to the northeast and a lower V_p/V_s feature to the west (Figure 11a). In Figure 11b, after correction using the residual gravity, the "aliased" bilobate feature in the original V_p/V_s variation is correctly resolved at the location of the Bloomfield Pluton. Ravat et al. (1987) have studied and modeled this pluton as a multidensity complex structure constrained by gravity and

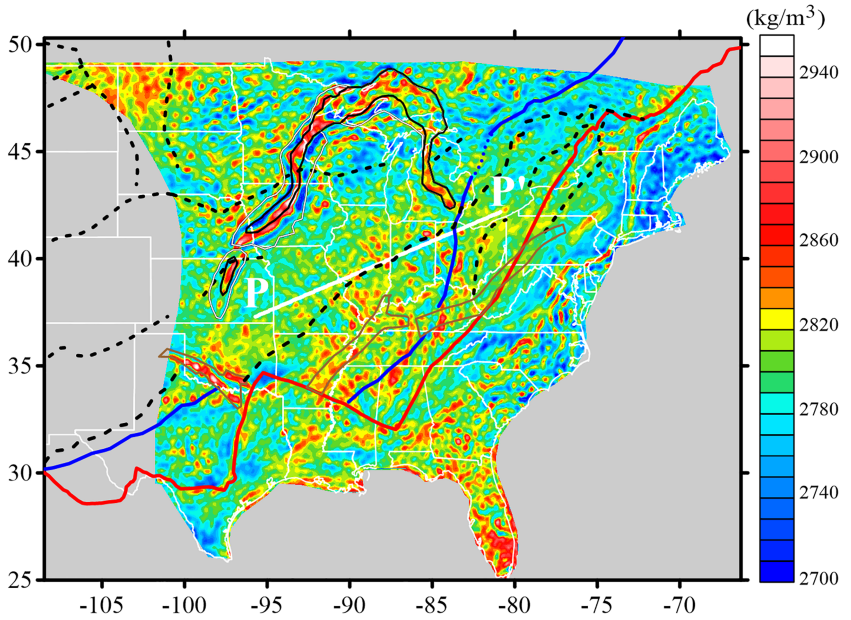

Figure 10. The corrected average density of the crystalline crust after inversion of <150 km wavelength residual gravity field in Figure 9b to density. The white line shows the profile across the deepest part of the Illinois basin analyzed in the discussion section.

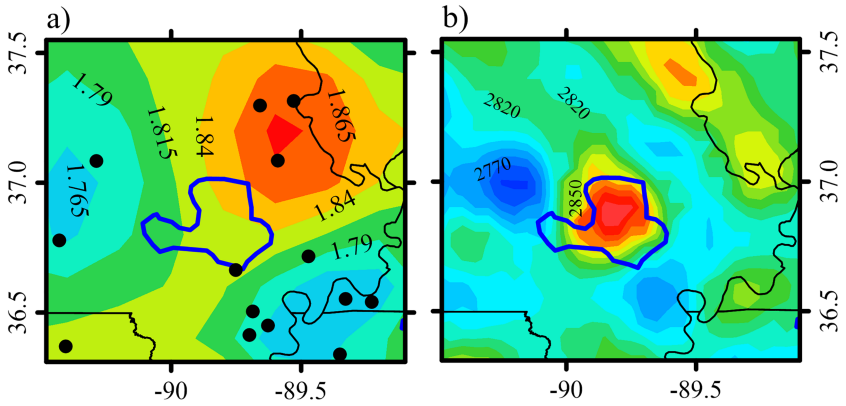

Figure 11. (a) The crustal V_p/V_s from Figure 3a and (b) the corrected crustal density (kg/m^3) from Figure 10. The pluton location is outlined in blue (Hildenbrand & Hendricks, 1995).

magnetic data gradients. They modeled a bulk density contrast of 100 kg/m^3 extending from the top of crystalline basement (2 km) to the base of the upper crust (17 km), with 6 km of additional denser material near its top in the central part of the pluton. The value we obtain in this study for the crustal average is consistent with the previously modeled density contrast of the pluton: the roughly 100 kg/m^3 density contrast in the upper 15 km of the crust, when distributed over a 40 km thick crust, is about 40 kg/m^3. The density contrast we obtain in this study after density correction is about 30–50 kg/m^3 (2,850–2,870 kg/m^3 for the bulk density of the pluton versus the average of about 2,820 kg/m^3 for the surrounding crust; Figure 11b).

It is reasonable to ask where else in the central and eastern United States the effects of aliasing and undersampling of crustal V_p/V_s might produce large discrepancies between the original and final crustal compositional anomalies similar to the above example of the Bloomfield Pluton. We illustrate the potential areas using a moving window estimate of correlation coefficients between the seismically derived crustal V_p/V_s and the corrected density model (Figure 12). The low and negative correlation coefficients on the map indicate areas where V_p/V_s variation may be aliased significantly by USArray sampling, especially where there

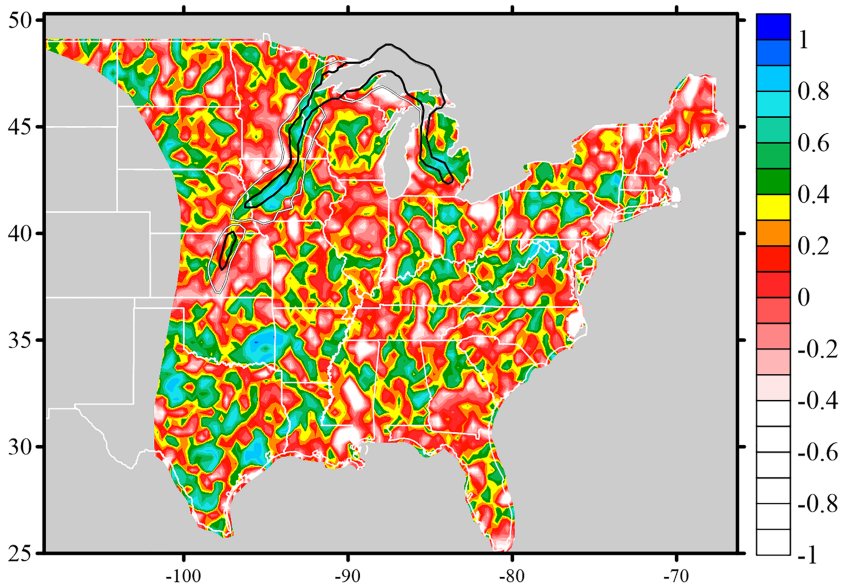

Figure 12. Moving window correlation coefficients between the crustal V_p/V_s and our corrected density model on the PACES gravity observation footprint using a window size of 1° by 1° and window offset of 0.3°. More than 85% of correlation coefficients are statistically significant (i.e., level of significance, $p < 0.05$).

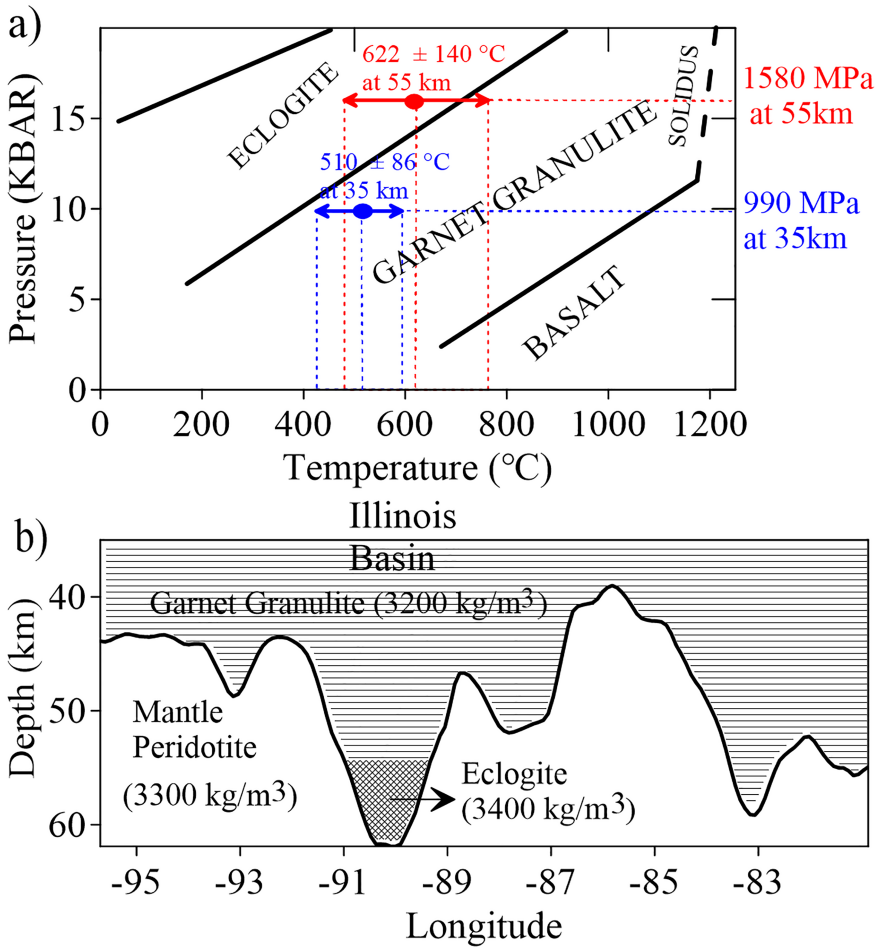

Figure 13. (a) A simplified diagram of gabbro-garnet granulite-eclogite phase changes from Ahrens and Schubert (1975) with pressure- and temperature-dependent phase transitions overlain by the central and eastern U.S. physical state. (b) A profile of the Moho depth variation crossing the Illinois basin, shown by the white line in Figure 10. The Moho depth along the profile is from Yang et al. (2017). The expected rock types according to the phase transitions in part (a) are indicated.

are significant gravity anomalies with wavelengths <70 km (e.g., faults and igneous plutons aligned along rifts or suture zones). The areas of relatively high correlation, on the other hand, suggest that the V_p/V_s variation is capturing the geologic variation observable in the gravity field. The map area exhibiting low and negative correlations is large, but not every low or negative correlation coefficient feature is expected to be meaningful from the point of view of tectonic interpretation. Some of the V_p/V_s variation also reflects longer-wavelength crustal variations not obvious in the density variation. However, some of these features do point to areas where V_p/V_s is undersampled and may lead to misinterpretation. As one example, we point to the location of the Grenville Front in Ohio, the eastern side of which shows low and negative correlations. Similarly, parts of the Midcontinent Rift in Kansas are undersampled/aliased as are parts of gravity highs in Ohio interpreted by Stein et al. (2018) as the eastern continuation of the Midcontinent Rift. Our study does not provide critical information, such as the ages of mafic rocks or the detailed structure of the crust, needed to answer questions regarding the hypothesis of the rift continuation. In the area of the Fort Wayne Rift, however, crustal densities (Figure 10) do not form a continuous zone of high density that is ubiquitously associated with the Midcontinent Rift. Additional higher spatial resolution experiments, including seismic refraction and reflection experiments, are necessary to understand better the crustal structure as it relates to these issues.

Other features of the density field estimates can be useful to interpret phase dynamics of the region. Along a profile through the thickest crust in the Illinois basin and the Granite-Rhyolite province (the Line PP′ in Figure 10), we estimate temperatures to be 510 ± 86 °C at 35 km depth and 622 ± 140 °C at 55 km, based

on a conductive thermal model combining surface heat flow and mineral physics of Pn seismic velocity (Ma & Lowry, 2017; Schutt et al., 2018). Corresponding pressures would be 990 and 1,580 MPa, respectively, assuming 15 km of granitic upper crust (2,750 kg/m^3) underlain by gabbro (3,000 kg/m^3). We combine this pressure-temperature information with the gabbro-garnet granulite-eclogite phase diagram from Ahrens and Schubert (1975) (Figure 13a). The phase relations imply garnet granulite (with a density of 3,200 kg/m^3, Ito & Kennedy, 1970) at depths between 35 and 55 km, with possible eclogitic lower crust below 55 km (Figure 13b). This may explain low Pn velocity observed in the New Madrid region of southern Illinois (Buehler & Shearer, 2017) if the tomographic inversion misinterpreted eclogitic lower crust as the top of mantle (and it would also imply Moho temperatures are overestimated in that region). Thus, much of the crust below 35 km may have only about +100 kg/m^3 density contrast (from lower crust to mantle). Moreover, in parts of the Illinois Basin where the Moho is deeper than 55 km, eclogite in the lowermost crust may result in a density contrast of −100 kg/m^3 (i.e., higher density in the lower crust). These low regional values of density contrasts are likely contributing to the lower-than-expected average Moho density contrast we observe in the central and eastern United States.

5. Conclusions

In this study, we augment an intracrustal density model constructed from joint inversion of seismic receiver function and gravity by inverting residual gravity anomalies that are aliased by USArray seismic station spacing for smaller-scale variations in V_p/V_s and density of the crust. We show, using the example of the Bloomfield Pluton in the midcontinent, that including shorter-wavelength content of the gravity anomalies corrects the "aliased" variation in crustal V_p/V_s and centers the density anomaly within the pluton's boundaries. We also show that density variations from sedimentary basin thickness, crustal thickness, crustal V_p/V_s, and upper mantle V_p/V_s do not explain fully the observed gravity field; however, crustal density variation constrained by seismic information is useful for separating crustal and mantle contributions to gravity.

The low Moho density contrast of 110 kg/m^3 determined for the central and eastern United States is lower than earlier inferences of low Moho density contrast from receiver function models derived from EarthScope data (e.g., 172 kg/m^3 for the eastern United States in Ma & Lowry, 2017), but it can be justified by lower crustal garnet granulite and eclogite in the deepest part of the crust. In the central and eastern United States, the lower crustal shear velocity and V_p/V_s are approximately 4.0 km/s (Gaherty et al., 2009) and 1.88 (Ma, 2017), respectively, which indicates the presence of garnet granulite in the lower crust having densities closer to the higher end of the range (~3,000–3,215 kg/m^3, Christensen, 1996). Our very low average value for a mantle V_p/V_s-density relationship (30 kg/m^3, which indicates no relationship for all practical purposes) for the central and eastern United States is also consistent with the few available laboratory measurements on unaltered mantle peridotites and pyroxenites, which show only uncorrelated scatter at best.

Appendix A: Minimization of RMS Residual Between Observed and Modeled Gravity to Determine Moho Density Contrast

We performed correlation tests to assess potential bias error in estimates of the Moho density contrast using the RMS of the residual gravity. In the central and eastern United States, the correlation coefficient between the observed gravity and crustal V_p/V_s is 0.11; the observed gravity and the crustal thickness is −0.47, and the crustal thickness and the crustal V_p/V_s is 0.21. We created a synthetic model with similar correlation properties and a Moho variation with a density contrast of 110 kg/m^3, equivalent to our estimate obtained in the study, except where the crustal thickness variation has a correlation coefficient of 0.48. We then used a range of Moho density contrasts and computed the RMS between the observed and computed gravity anomalies and the correlation coefficients. The tests shown in Figure A1 indicate that the minimum value of the RMS of the gravity residual has low correlation coefficient and it is able to determine the Moho density contrast when the crustal V_p/V_s correlates poorly with the crustal thickness; for example, it results in 105 kg/m^3 when the correlation coefficient is 0.21. Alternatively, when crustal V_p/V_s correlates strongly with the crustal thickness, that would bias estimates of the Moho density contrast.

In the central and eastern United States, the crustal V_p/V_s has a low correlation coefficient with the crustal thickness of 0.14. Thus, we expect that our estimate of the Moho density contrast is accurate as suggested in Figure A1e.

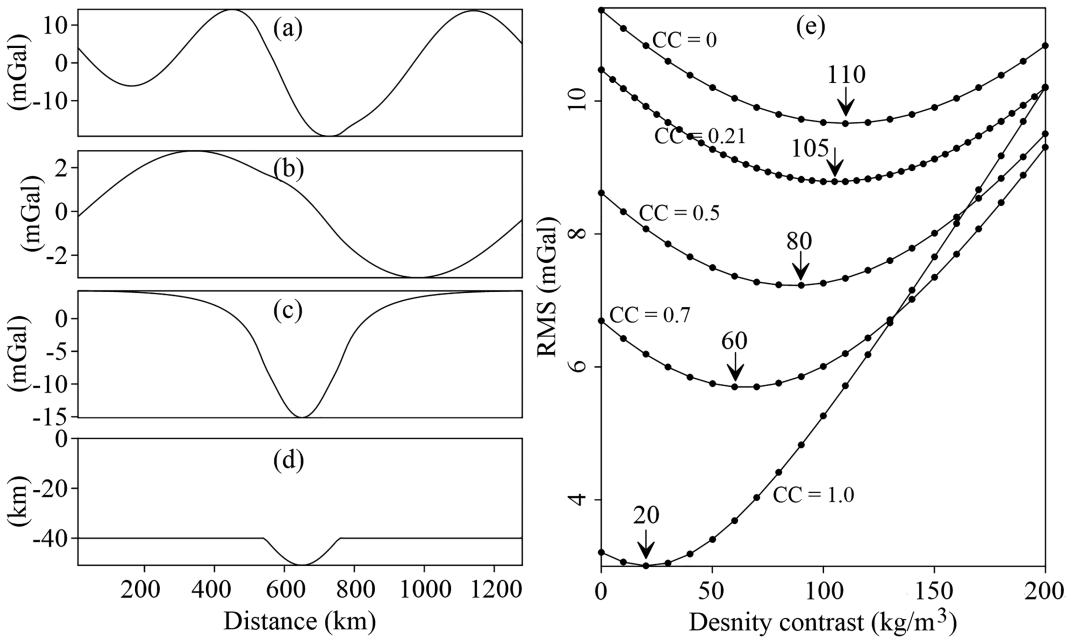

Figure A1. Synthetic test based on the data information from the central and eastern United States. (a) Observed gravity anomaly. (b) Gravity effect from the crustal V_p/V_s. (c) Gravity effect from the crustal thickness with a density contrast of 110 kg/m^3. (d) Crustal thickness. (e) The estimated Moho density contrasts from different correlation coefficients between the crustal *Vp/Vs* and the crustal thickness using the approach stated in the manuscript.

Acknowledgments
The crustal density data set generated for this research is publicly available at Zhang et al. (2019). Continental U.S. Bouguer gravity data used in the study were downloaded from the Pan-American Center for Earth and Environmental Studies (PACES). The seismic refraction data set used in the study was provided by Dr. Walter Mooney, and the sedimentary thickness data set used for comparison purposes was provided by Dr. Mikhail Kaban. Dr. Ellett of Indiana Geological Survey provided the Illinois basin sedimentary thickness data, and Dr. Hickman of Kentucky Geological Survey provided the Rome Trough sedimentary thickness data. We also benefitted from the CRUST1.0 model of Laske et al. and the Bouguer gravity data from "Bureau Gravimétrique International (BGI, http://bgi.obs-mip.fr)." We thank William J. Hinze and one anonymous reviewer for their assistance in reviewing this manuscript. This work was motivated and supported by the U. S. National Science Foundation Awards 1246921 and 1246977 to D. R. and A. R. L. It was also financially supported in part by the National Nature Science Foundation of China (41604121), and the Laboratory for Marine Geology, Qingdao National Laboratory for Marine Science and Technology (MGQNLM201708).

References

Ahrens, T. J., & Schubert, G. (1975). Gabbro-eclogite reaction rate and its geophysical significance. *Reviews of Geophysics*, *13*(2), 383–400. https://doi.org/10.1029/RG013i002p00383

Barton, P. J. (1986). The relationship between seismic velocity and density in the continental crust—A useful constraint? *Geophysical Journal International*, *87*(1), 195–208. https://doi.org/10.1111/j.1365-246X.1986.tb04553.x

Bechtel, T. D., Forsyth, D. W., Sharpton, V. L., & Grieve, R. A. (1990). Variations in effective elastic thickness of the North American lithosphere. *Nature*, *343*(6259), 636–638. https://doi.org/10.1038/343636a0

Bedrosian, P. A. (2016). Making it and breaking it in the Midwest: Continental assembly and rifting from modeling of EarthScope magnetotelluric data. *Precambrian Research*, *278*, 337–361. https://doi.org/10.1016/j.precamres.2016.03.009

Birch, F. (1960). The velocity of compressional waves in rocks to 10 kilobars, Part 1. *Journal of Geophysical Research*, *65*(4), 1083–1102. https://doi.org/10.1029/JZ065i004p01083

Birch, F. (1961). The velocity of compressional waves in rocks to 10 kilobars. Part 2. *Journal of Geophysical Research*, *66*(7), 2199–2224. https://doi.org/10.1029/JZ066i007p02199

Biryol, C. B., Wagner, L. S., Fischer, K. M., & Hawman, R. B. (2016). Relationship between observed upper mantle structures and recent tectonic activity across the Southeastern United States. *Journal of Geophysical Research: Solid Earth*, *121*, 3393–3341. https://doi.org/10.1002/2015JB012698

Brocher, T. M. (2005). Empirical relations between elastic wavespeeds and density in the Earth's crust. *Bulletin of the Seismological Society of America*, *95*(6), 2081–2092. https://doi.org/10.1785/0120050077

Buehler, J. S., & Shearer, P. M. (2016). Characterizing earthquake location uncertainty in North America using source–receiver reciprocity and USArray. *Bulletin of the Seismological Society of America*, *106*(5), 2395–2401. https://doi.org/10.1785/0120150173

Buehler, J. S., & Shearer, P. M. (2017). Uppermost mantle seismic velocity structure beneath USArray. *Journal of Geophysical Research: Solid Earth*, *122*, 436–448. https://doi.org/10.1002/2016JB013265

Cammarano, F., Goes, S., Vacher, P., & Giardini, D. (2003). Inferring upper-mantle temperatures from seismic velocities. *Physics of the Earth and Planetary Interiors*, *138*(3-4), 197–222. https://doi.org/10.1016/S0031-9201(03)00156-0

Caratori Tontini, F., Cocchi, L., & Carmisciano, C. (2008). Potential-field inversion for a layer with uneven thickness: The Tyrrhenian Sea density model. *Physics of the Earth and Planetary Interiors*, *166*(1-2), 105–111. https://doi.org/10.1016/j.pepi.2007.10.007

Catchings, R. D. (1999). Regional Vp, Vs, *Vp/Vs* and Poisson's ratios across earthquake source zones from Memphis, TN, to St. Louis, MO. *Bulletin of the Seismological Society of America*, *89*(6), 1591–1605.

Christensen, N. I. (1996). Poisson's ratio and crustal seismology. *Journal of Geophysical Research*, *101*(B2), 3139–3156. https://doi.org/10.1029/95JB03446

Christensen, N. I., & Mooney, W. D. (1995). Seismic velocity structure and composition of the continental crust: A global view. *Journal of Geophysical Research*, *100*(B6), 9761–9788. https://doi.org/10.1029/95JB00259

Crotwell, H. P., & Owens, T. J. (2005). Automated receiver function processing. *Seismological Research Letters*, *76*(6), 702–709. https://doi.org/10.1785/gssrl.76.6.702

Ellett, K. M., & Naylor, S. (2016). *Utility of geological and pedological models in the design of geothermal heat pump systems* (Vol. 519, SPE519-01). Boulder: Geological Society of America, *Special Papers*.

Frassetto, A. M., Zandt, G., Gilbert, H., Owens, T. J., & Jones, C. H. (2011). Structure of the Sierra Nevada from receiver functions and implications for lithospheric foundering. *Geosphere*, *7*(4), 898–921. https://doi.org/10.1130/GES00570.1

Gaherty, J. B., Dalton, C., & Levin, V. (2009). Three-dimensional models of crustal structure in eastern North America, USGS Technical Report. https://www.ldeo.columbia.edu/~gaherty/CEUS_Model.html

Heeszel, D. S., Wiens, D. A., Anandakrishnan, S., Aster, R. C., Dalziel, I. W., Huerta, A. D., et al. (2016). Upper mantle structure of central and West Antarctica from array analysis of Rayleigh wave phase velocities. *Journal of Geophysical Research: Solid Earth*, *121*, 1758–1775. https://doi.org/10.1002/2015JB012616

Hildenbrand, T. G., & Hendricks, J. D. (1995). *Geophysical setting of the Reelfoot rift and relations between rift structures and the New Madrid seismic zone*, *Professional Paper* (Vol. 1538-E). Denver: U.S. Geological Survey.

Hinze, W. J., Wold, R. J., & O'Hara, N. W. (1982). *10: Gravity and magnetic studies of Lake Superior*, *Memoirs* (Vol. 156, pp. 203–222). Boulder: Geological Society of America.

IRIS DMC (2010). Data Services Products: EARS EarthScope Automated Receiver Survey. https://doi.org/10.17611/DP/EARS.1

Ito, K., & Kennedy, G. (1970). *The fine structure of the basalt-eclogite transition*, *Special Papers* (Vol. 3, pp. 77–83). Boulder, CO: Mineralogical Society of America.

Ji, S. C., Wang, Q., & Xia, B. (2002). *Hand book of seismic properties of minerals, rocks and ores* (p. 630). Mont Real: Polytechnic International Press.

Kende, J., Henry, P., Bayrakci, G., Oeren, M. S., & Grall, C. (2017). Moho depth and crustal thinning in the Marmara Sea region from gravity data inversion. *Journal of Geophysical Research*, *122*, 1381–1401. https://doi.org/10.1002/2015JB012735

Kennett, B. L. N., Engdahl, E. R., & Buland, R. (1995). Constraints on seismic velocities in the earth from travel times. *Geophysical Journal International*, *122*(1), 108–124. https://doi.org/10.1111/j.1365-246X.1995.tb03540.x

Kirby, J. F., & Swain, C. J. (2009). A reassessment of spectral T_e estimation in continental interiors: The case of North America. *Journal of Geophysical Research*, *114*, B08401. https://doi.org/10.1029/2009JB006356

Kiser, E., Palomeras, I., Levander, A., Zelt, C., Schmandt, B., Hansen, S., et al. (2016). Magma reservoirs from the upper crust to the Moho inferred from high-resolution Vp and Vs models beneath Mount St. Helens, Washington State, USA. *Geology*, *44*(6), 411–414. https://doi.org/10.1130/G37591.1

Laske, G., Masters, G., Ma, Z., & Pasyanos, M. E. (2012). CRUST1.0: An updated global model of Earth's crust. *Geophysical Research Abstracts*, *14*, 3743.

Levin, V., VanTongeren, J. A., & Servali, A. (2016). How sharp is the sharp Archean Moho? Example from eastern Superior Province. *Geophysical Research Letters*, *43*, 1928–1933. https://doi.org/10.1002/2016GL067729

Liu, L., & Hasterok, D. (2016). High-resolution lithosphere viscosity and dynamics revealed by magnetotelluric imaging. *Science*, *353*(6307), 1515–1519. https://doi.org/10.1126/science.aaf6542

Long, M. D., Jackson, K. G., & McNamara, J. F. (2016). *SKS* splitting beneath Transportable Array stations in eastern North America and the signature of past lithospheric deformation. *Geochemistry, Geophysics, Geosystems*, *17*, 2–15. https://doi.org/10.1002/2015GC006088

Love, J. J., Pulkkinen, A., Bedrosian, P. A., Jonas, S., Kelbert, A., Rigler, E. J., et al. (2016). Geoelectric hazard maps for the continental United States. *Geophysical Research Letters*, *43*, 9415–9424. https://doi.org/10.1002/2016GL070469

Lowry, A. R., & Pérez-Gussinyé, M. (2011). The role of crustal quartz in controlling cordilleran deformation. *Nature*, *471*(7338), 353–357. https://doi.org/10.1038/nature09912

Ludwig, W. J., Nafe, J. E., & Drake, C. L. (1970). *Seismic refraction. The sea, 4 (Part 1)* (pp. 53–84). New York: Wiley-Interscience.

Ma, X. F., "USArray Imaging of North American Continental Crust" (2017), PhD Dissertation 6904. https://digitalcommons.usu.edu/etd/6904

Ma, X. F., & Lowry, A. R. (2017). USArray imaging of continental crust in the conterminous United States. *Tectonics*, *36*, 2882–2902. https://doi.org/10.1002/2017TC004540

McGlannan, A. J., & Gilbert, H. (2016). Crustal signatures of the tectonic development of the North American midcontinent. *Earth and Planetary Science Letters*, *433*, 339–349. https://doi.org/10.1016/j.epsl.2015.10.048

Miller, M. S., Zhang, P., & Dolan, J. F. (2014). Moho structure across the San Jacinto fault zone: Insights into strain localization at depth. *Lithosphere*, *6*(1), 43–47. https://doi.org/10.1130/L295.1

Mooney, W. D., Andrews, M. C., Ginzburg, A., Peters, D. A., & Hamilton, R. M. (1983). Crustal structure of the northern Mississippi embayment and a comparison with other continental rift zones. *Tectonophysics*, *94*(1-4), 327–348. https://doi.org/10.1016/0040-1951(83)90023-9

Mooney, W. D., & Kaban, M. K. (2010). The North American upper mantle: Density, composition, and evolution. *Journal of Geophysical Research*, *115*, B12424. https://doi.org/10.1029/2010JB000866

Nyamwandha, C. A., Powell, C. A., & Langston, C. A. (2016). A joint local and teleseismic tomography study of the Mississippi Embayment and New Madrid Seismic Zone. *Journal of Geophysical Research: Solid Earth*, *121*, 3570–3585. https://doi.org/10.1002/2015JB012761

Parker, E. H. (2013). *Vp/Vs* variations across terrane boundaries in the southern Appalachians: Implications for Alleghanian thin-skinned tectonic models. *GSA Abstracts with Programs*, *40*(15), 3853–3857.

Parker, R. L. (1973). The rapid calculation of potential anomalies. *Geophysical Journal International*, *31*(4), 447–455. https://doi.org/10.1111/j.1365-246X.1973.tb06513.x

Pollitz, F. F., & Mooney, W. D. (2016). Seismic velocity structure of the crust and shallow mantle of the Central and Eastern United States by seismic surface wave imaging. *Geophysical Research Letters*, *43*, 118–126. https://doi.org/10.1002/2015GL066637

Porter, R., Liu, Y., & Holt, W. E. (2016). Lithospheric records of orogeny within the continental US. *Geophysical Research Letters*, *43*, 144–153. https://doi.org/10.1002/2015GL066950

Ravat, D., Braile, L. W., & Hinze, W. J. (1987). Earthquakes and plutons in the midcontinent—Evidence from the bloomfield pluton, new madrid rift complex. *Seismological Research Letters*, *58*(2), 41–52. https://doi.org/10.1785/gssrl.58.2.41

Ravat, D., Lu, Z., & Braile, L. W. (1999). Velocity–density relationships and modeling the lithospheric density variations of the Kenya Rift. *Tectonophysics*, *302*(3-4), 225–240. https://doi.org/10.1016/S0040-1951(98)00283-2

Savage, B., Covellone, B. M., & Shen, Y. (2016). Wave speed structure of the eastern North American margin. *Earth and Planetary Science Letters*, *459*, 394–405. https://doi.org/10.1016/j.epsl.2016.11.028

Schmandt, B., & Humphreys, E. (2010). Complex subduction and small-scale convection revealed by body-wave tomography of the western United States upper mantle. *Earth and Planetary Science Letters*, *297*(3-4), 435–445. https://doi.org/10.1016/j.epsl.2010.06.047

Schmandt, B., & Lin, F. C. (2014). *P* and *S* wave tomography of the mantle beneath the United States. *Geophysical Research Letters*, *41*, 6342–6349. https://doi.org/10.1002/2014GL061231

Schmandt, B., Lin, F. C., & Karlstrom, K. E. (2015). Distinct crustal isostasy trends east and west of the Rocky Mountain Front. *Geophysical Research Letters*, *42*, 10,290–10,298. https://doi.org/10.1002/2015GL066593

Schutt, D. L., Lowry, A. R., & Buehler, J. S. (2018). Moho temperature and mobility of lower crust in the western United States. *Geology*, *46*(3), 219–222. https://doi.org/10.1130/G39507.1

Shen, W., & Ritzwoller, M. H. (2016). Crustal and uppermost mantle structure beneath the United States. *Journal of Geophysical Research: Solid Earth*, *121*, 4306–4342. https://doi.org/10.1002/2016JB012887

Stanciu, A. C., Russo, R. M., Mocanu, V. I., Bremner, P. M., Hongsresawat, S., Torpey, M. E., et al. (2016). Crustal structure beneath the Blue Mountains terranes and cratonic North America, eastern Oregon, and Idaho, from teleseismic receiver functions. *Journal of Geophysical Research: Soild Earth*, *121*, 5049–5067. https://doi.org/10.1002/2016JB012989

Stein, S., Stein, C. A., Elling, R., Kley, J., Keller, G. R., Wysession, M., et al. (2018). Insights from North America's failed Midcontinent Rift into the evolution of continental rifts and passive continental margins. *Tectonophysics*, *744*, 403–421. https://doi.org/10.1016/j.tecto.2018.07.021

Tape, C., Plesch, A., Shaw, J. H., & Gilbert, H. (2012). Estimating a continuous Moho surface for the California unified velocity model. *Seismological Research Letters*, *83*(4), 728–735. https://doi.org/10.1785/0220110118

Thurner, S., Margolis, R., Levander, A., & Niu, F. (2015). PdS receiver function evidence for crustal scale thrusting, relic subduction, and mafic underplating in the Trans-Hudson Orogen and Yavapai province. *Earth and Planetary Science Letters*, *426*, 13–22. https://doi.org/10.1016/j.epsl.2015.06.007

Van Schmus, W. R., & Hinze, W. J. (1985). The Midcontinent Rift system. *Annual Review of Earth and Planetary Sciences*, *13*(1), 345–383. https://doi.org/10.1146/annurev.ea.13.050185.002021

Wang, Q., Bagdassarov, N., & Ji, S. C. (2013). The Moho as a transition zone: A revisit from seismic and electrical properties of minerals and rocks. *Tectonophysics*, *609*, 395–422. https://doi.org/10.1016/j.tecto.2013.08.041

Whitmeyer, S. J., & Karlstrom, K. E. (2007). Tectonic model for the Proterozoic growth of North America. *Geosphere*, *3*(4), 220–259. https://doi.org/10.1130/GES00055.1

Workman, E., Lin, F. C., & Koper, K. D. (2017). Determination of Rayleigh wave ellipticity across the Earthscope Transportable Array using single-station and array-based processing of ambient seismic noise. *Geophysical Journal International*, *208*(1), 234–245. https://doi.org/10.1093/gji/ggw381

Yang, X. T., Pavlis, G. L., Hamburger, M. W., Marshak, S., Gilbert, H., Rupp, J., et al. (2017). Detailed crustal thickness variations beneath the Illinois Basin area: Implications for crustal evolution of the midcontinent. *Journal of Geophysical Research: Solid Earth*, *122*, 6323–6345. https://doi.org/10.1002/2017JB014150

Yeck, W. L., Sheehan, A. F., & Schulte-Pelkum, V. (2013). Sequential H-K stacking to obtain accurate crustal thicknesses beneath sedimentary basins. *Bulletin of the Seismological Society of America*, *103*(3), 2142–2150. https://doi.org/10.1785/0120120290

Yuan, H., Dueker, K., & Stachnik, J. (2010). Crustal structure and thickness along the Yellowstone hot spot track: Evidence for lower crustal outflow from beneath the eastern Snake River Plain. *Geochemistry, Geophysics, Geosystems*, *11*, Q03009. https://doi.org/10.1029/2009GC002787

Zhang, H. L., Ravat, D., & Lowry, A. R. (2019). Crustal density variation of the eastern U.S., archived at https://uknowledge.uky.edu/ees_data/1/. https://doi.org/10.13023/ve6j-re17